Electronic Supplementary Material (ESI) for Journal of Materials Chemistry A.

Supporting Information

Perovskite Solar Cells Employing an Eco-friendly and Low-cost Inorganic Hole Transport Layer for Enhanced Photovoltaic Performance and Operational Stability

Xin Li,[1] Junyou Yang,*,[1] Qinghui Jiang,[1] Hui Lai,[1,2] Shuiping Li,[1] Yao Tan [1], Ying Chen [1] and Suwei Li [1]

1. State Key Laboratory of Material Processing and Die & Mould Technology, Huazhong University of Science and Technology, Wuhan 430074, P.R. China.

E-mail: *jyyang@mail.hust.edu.cn*.

2. China-Eu Institute for Clean and Renewable Energy, Huazhong University of Science and Technology, Wuhan 430074, P.R. China

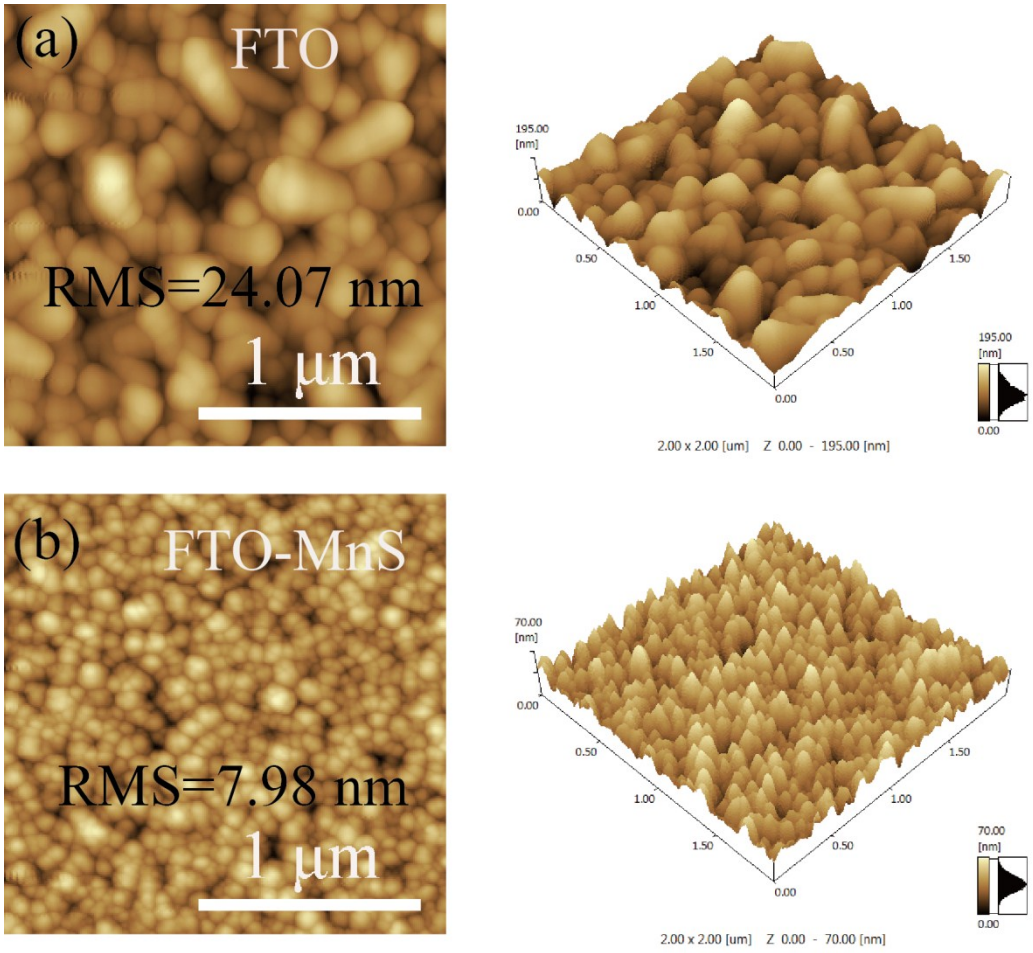

Figure S1. AFM images for (a) FTO and (b) vapor-deposited MnS film on FTO substrate.

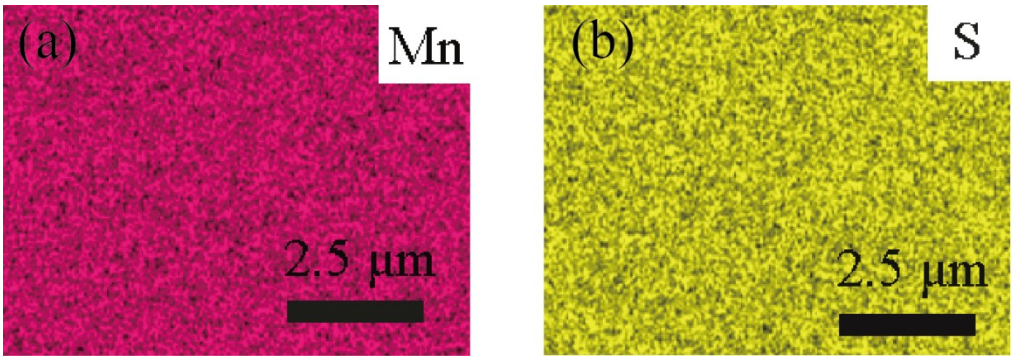

Figure S2. EDS mappings of (a) Mn and (b) S content.

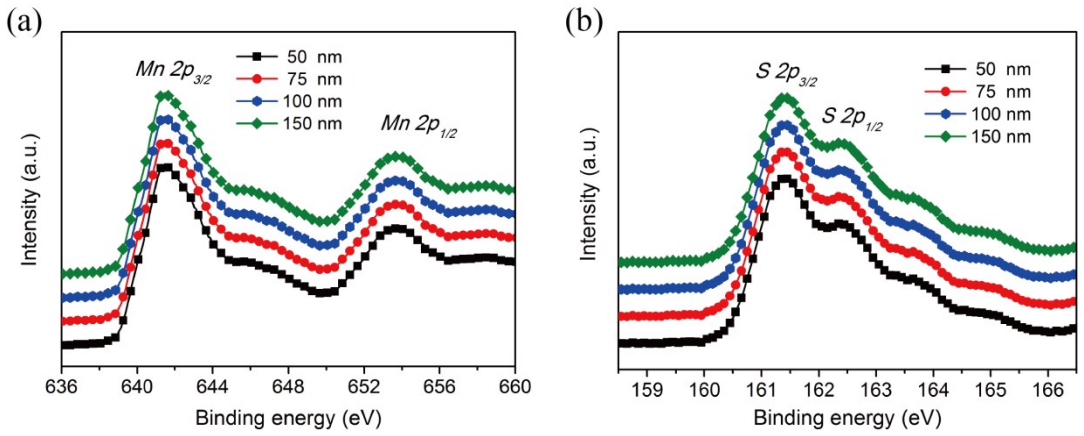

Figure S3. XPS spectra of the MnS film with deposition thickness of 50, 75, 100, and 150 nm: (a) Mn 2p and (b) S 2p core levels.

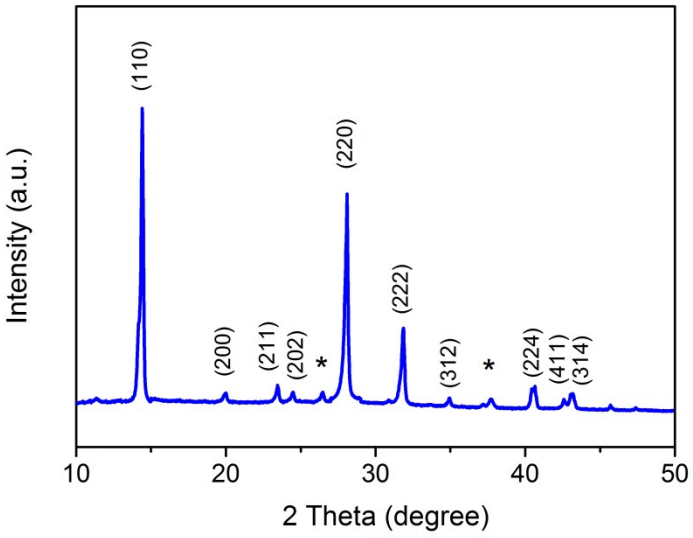

Figure S4. XRD pattern of the perovskite film fabricated in this work.

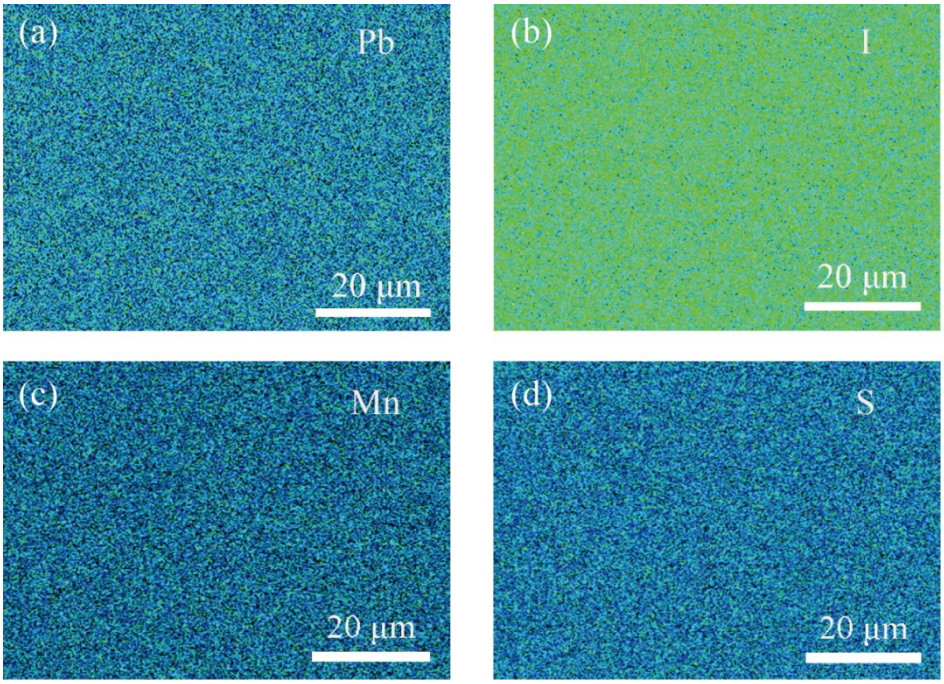

Figure S5. EPMA images of MnS deposited on perovskite layer for (a) Pb, (b) I, (c) Mn and (d) S content.

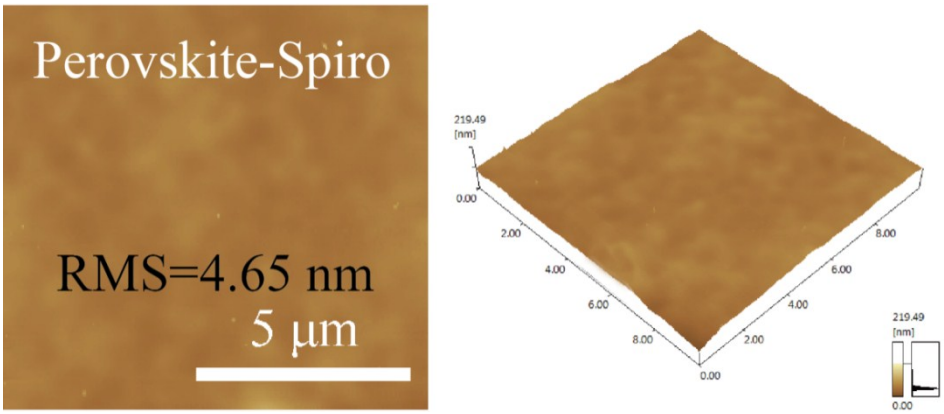

Figure S6. AFM images for Spiro-OMeTAD HTL on perovskite layer.

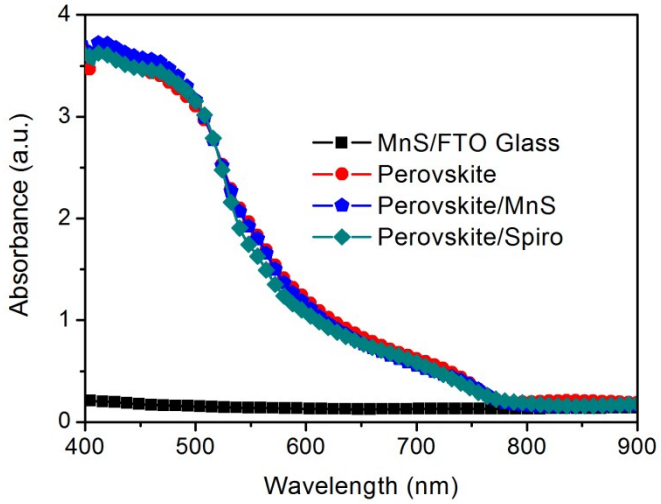

Figure S7. Absorption spectra of the MnS film, perovskite film, and perovskite film with different HTLs.

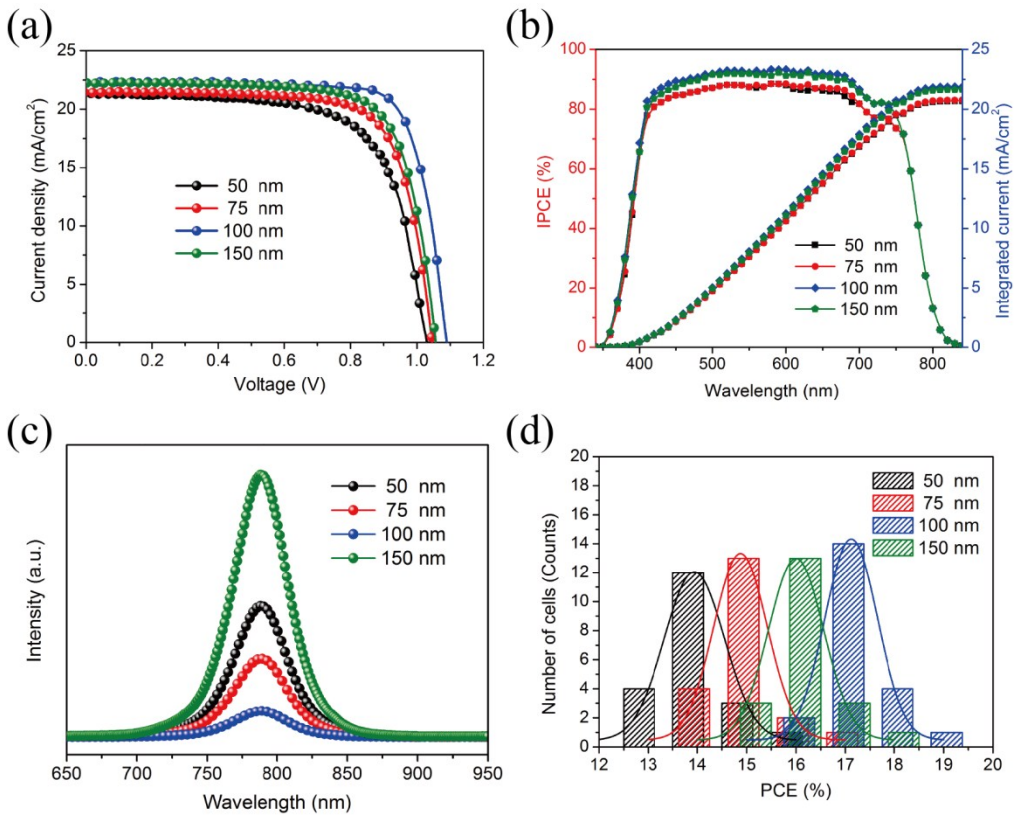

Figure S8. (a) *J-V* curves of the perovskite solar cells based on various MnS HTLs. (b) IPCE spectra of various MnS HTLs based PKSCs. (c) Steady-state PL spectra of the perovskite films based on different MnS films. (d) Histograms of PCEs for 20 cells with various MnS HTLs measured under reverse voltage scan, respectively.

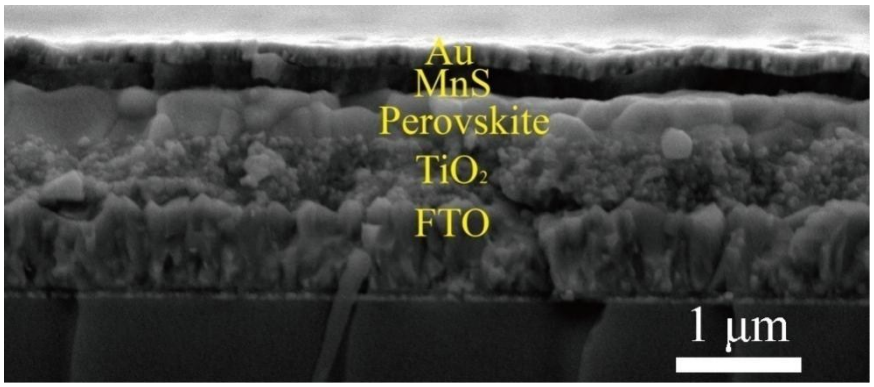

Figure S9. Cross-sectional SEM images of the studied device.

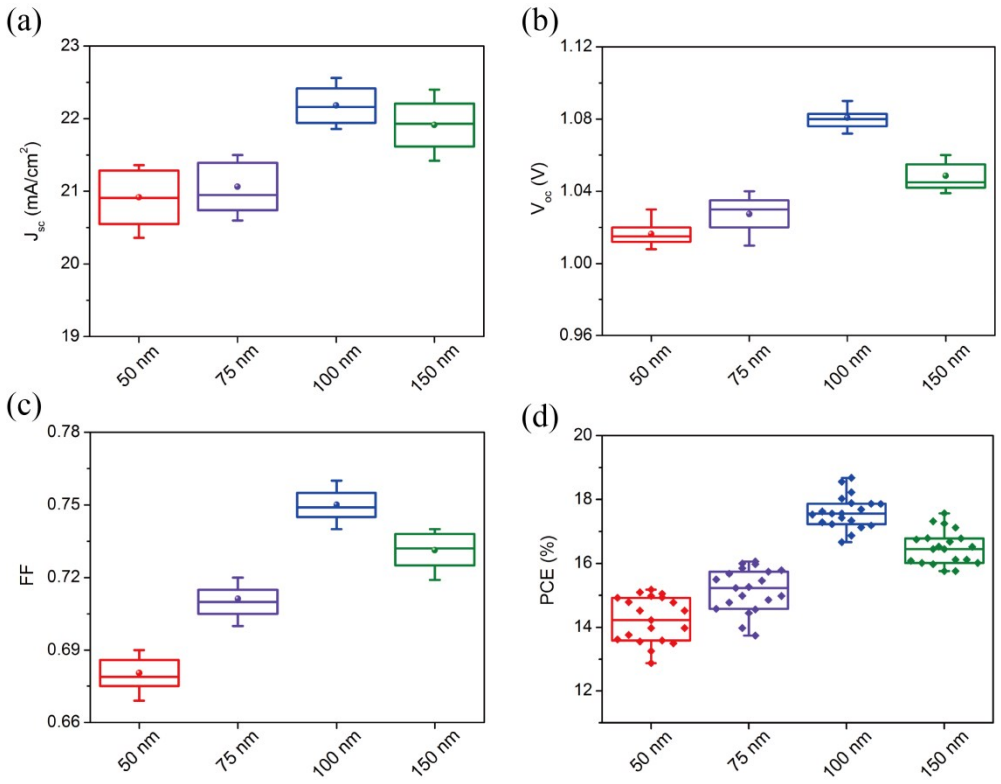

Figure S10. Box chart of photovoltaic parameters comparison of perovskite solar cells based on MnS with various deposition thickness. The data were statistically analyzed from 20 cells per sample type (deposition thickness). (a) J_{sc} (mA/cm^2), (b) V_{oc} (V), (c) *FF*, (d) PCE (%).

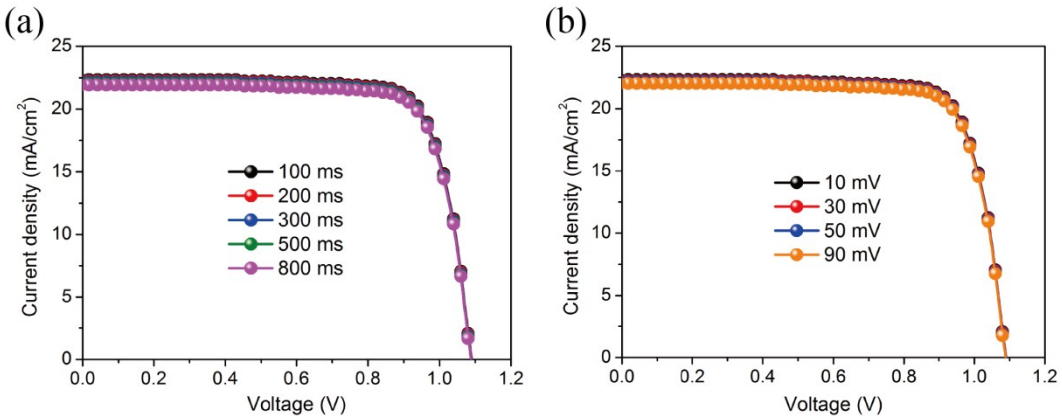

Figure S11. *J-V* curves of the sample device based on MnS HTL with (a) different step delay times (at 50 mV voltage step size) and (b) voltage step sizes (at 500 ms step delay time).

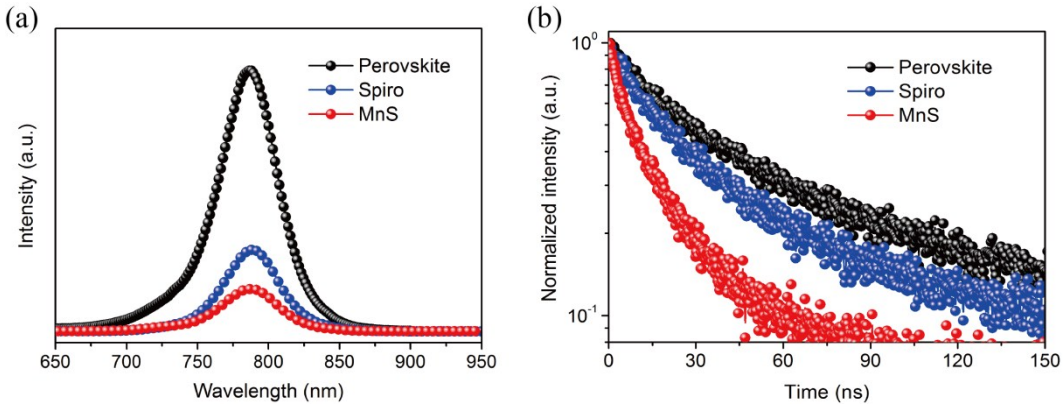

Figure S12. (a) Steady-state PL spectra and (b) time-resolved PL spectra of Spiro and MnS based on perovskite film.

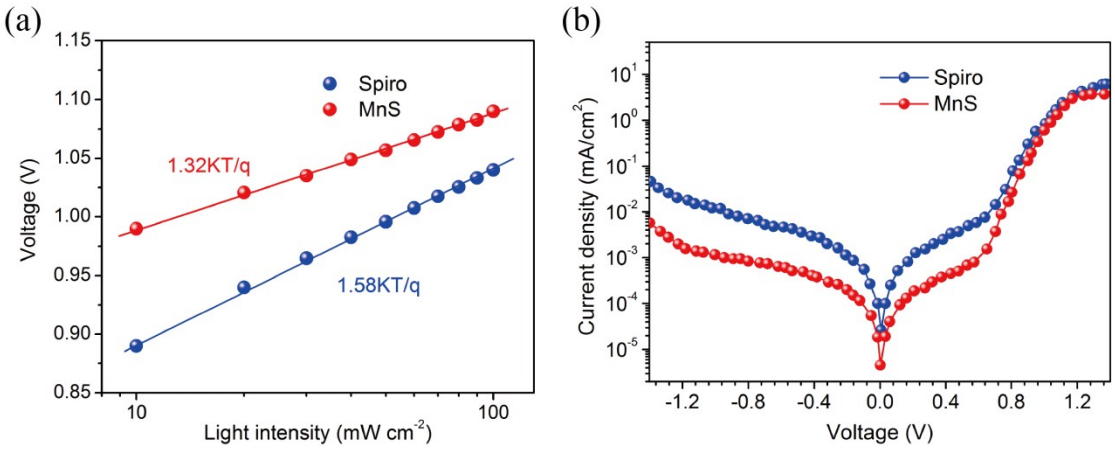

Figure S13. (a) The dependence of V_{oc} on different light intensity for the optimized MnS based device and the control device. (b) The dark *J*-*V* curves of the optimized devices based on Spiro and MnS HTLs, respectively.

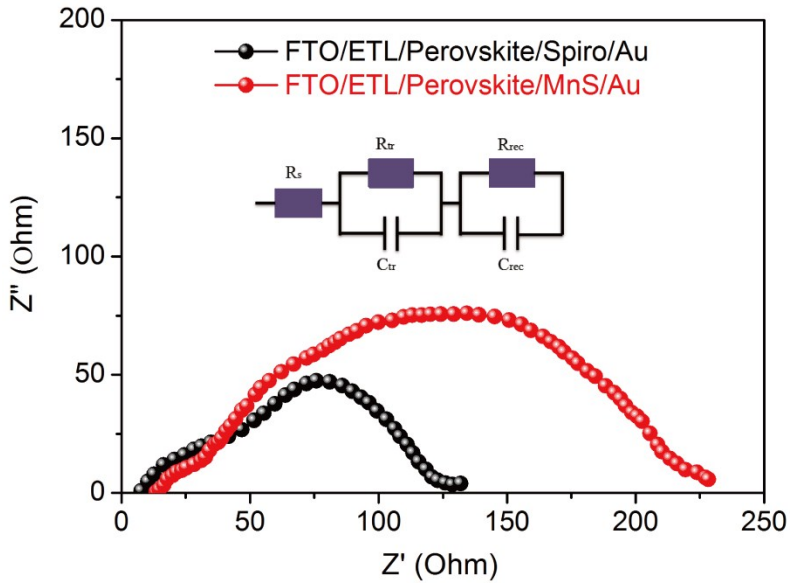

Figure S14. Nyquist plots of the EIS for the PKSC devices based on Spiro and MnS HTL under illumination at around open-circuit voltage.

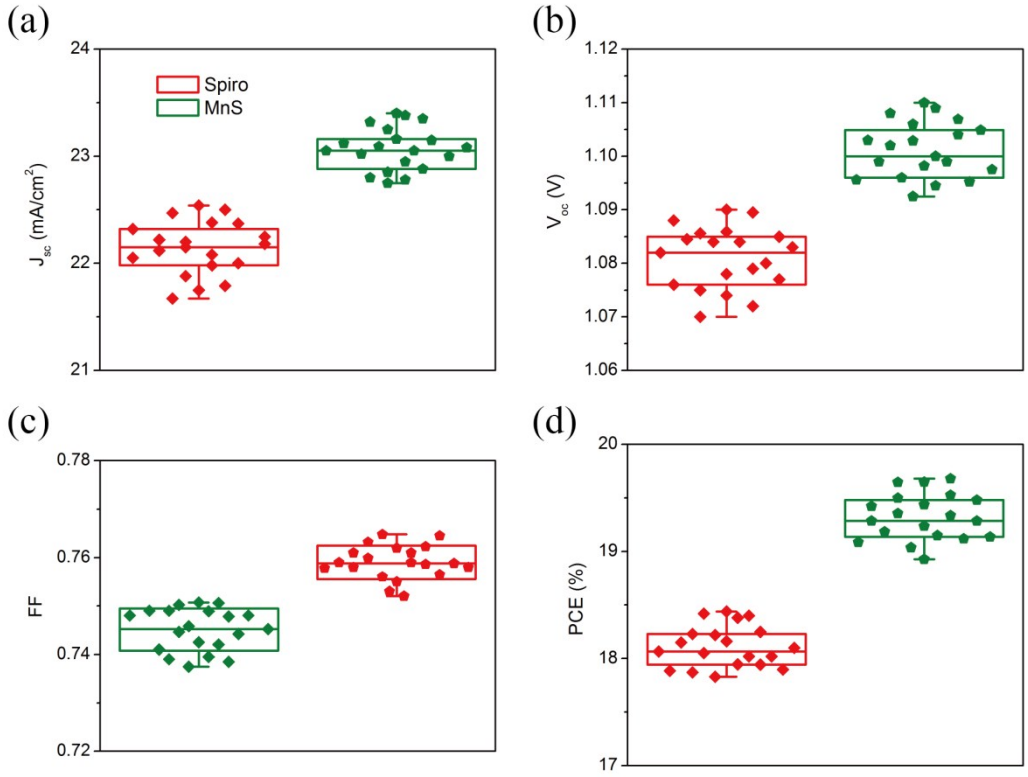

Figure S15. Box chart of photovoltaic parameters comparison of mixed-perovskite solar cells based on Spiro and MnS, respectively. The data were statistically analyzed from 20 cells per sample type (deposition). (a) J_{sc} (mA/cm^2), (b) V_{oc} (V), (c) *FF*, (d) PCE (%).

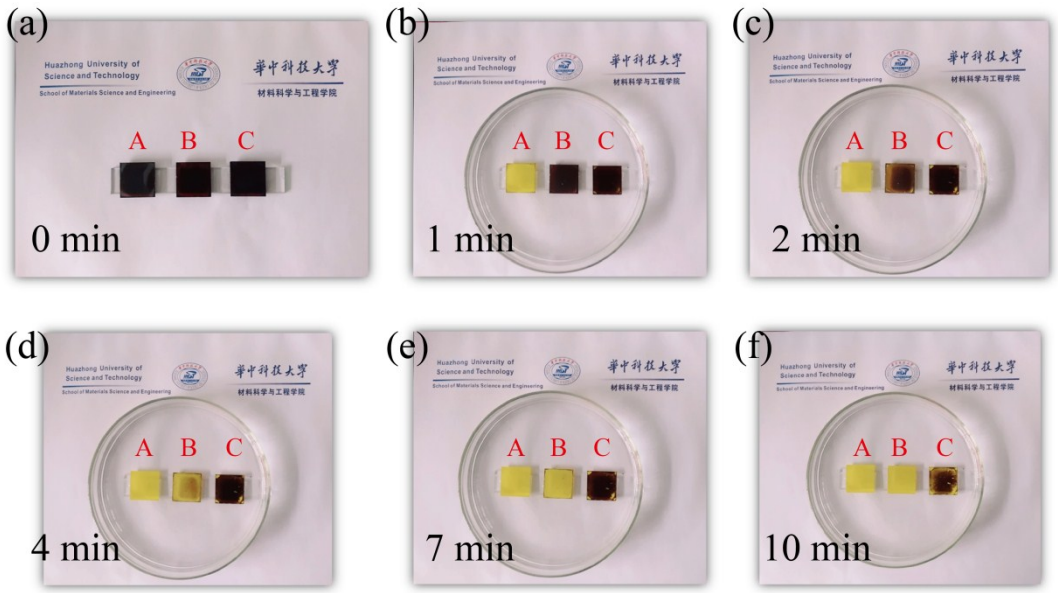

Figure S16. Comparison on the waterproof capability of different HTLs by immersing the films directly in water for about 10 minutes. Perovskite films without and with different HTLs covering on top have been compared. Sample A: Bare perovskite film, Sample B: Perovskite/Spiro-OMeTAD, and Sample C: Perovskite/MnS. Please note that: the color changed from dark brown to light yellow, reflecting the decomposition of perovskite to PbI_2.

Table S1. The best photovoltaic parameters the perovskite solar cells based on MnS layer with various thicknesses in the device architecture of FTO/c-TiO_2/m-TiO_2/$MAPbI_3$/MnS/Au.

Thickness (nm)	V_{oc} *(V)*	J_{sc} *(mA cm^{-2})*	*FF*	*η (%)*
50	1.03	21.36	0.69	15.18
75	1.04	21.45	0.72	16.06
100	1.09	22.56	0.76	18.68
150	1.06	22.40	0.74	17.57

Table S2. Photovoltaic performance of perovskite solar cells based on MnS and Spiro-OMeTAD HTLs.

Device	*Scan direction*	V_{oc} *(V)*	J_{sc} *(mA cm^{-2})*	*FF*	η *(%)*
Spiro	*Reverse*	1.04	22.24	0.74	17.12
	Forward	1.01	21.94	0.73	16.18
MnS	*Reverse*	1.09	22.56	0.76	18.68
	Forward	1.08	22.42	0.75	18.16

Table S3. Average photovoltaic parameters of the perovskite solar cells based on Spiro and MnS HTLs for 20 separated devices, respectively.

Sample	V_{oc} *(V)*	J_{sc} *(mA cm^{-2})*	*FF*	*η (%)*
Spiro	1.03±0.0072	21.37±0.309	0.73±0.0089	16.46±0.23
MnS	1.08±0.0050	21.94±0.317	0.75±0.0048	18.33±0.21

Table S4. PL decay curves of perovskite films based on Spiro and MnS well fitted by a bi-exponential decay kinetics equation:

PL intensity=$A_1\exp(-t/\tau_1)+A_2\exp(-t/\tau_2)$, and $\tau_{avg}=\tau_1\times(A_1/A_1+A_2)+\tau_2\times(A_2/A_1+A_2)$.

Sample name	A_1	τ_1(ns)	A_2	τ_2(ns)	τ_{avg}
Perovskite	33.2	11.22	66.8	56.35	41.36
Spiro HTL	57.4	16.28	42.6	58.91	34.44
MnS HTL	51.5	5.32	48.5	24.05	14.40

Table S5. Comparison on the hole mobility of MnS HTL and Spiro HTL.

Sample	*Hole mobility ($cm^2 V^{-1} s^{-1}$)*	*Conductivity ($S cm^{-1}$)*
MnS	4.50×10^{-1}	7.32×10^{-3}
Spiro	1.38×10^{-4}	5.64×10^{-4}

Table S6. The champion parameters of PKSC with various inorganic HTLs in n-i-p structure.

HTM	Perovskite	*Jsc*	*Voc*	*FF*	*PCE*	Ref
CuI	$MAPbI_3$	22.78	1.03	0.75	17.60	1
Cu_2ZnSnS_4	$MAPbI_3$	20.54	1.06	0.59	12.75	2
Cu_2O	$MAPbI_{3-x}Cl_x$	15.80	0.96	0.59	8.93	3
$CuGaO_2$	$MAPbI_{3-x}Cl_x$	21.66	1.11	0.77	18.51	4
CuSCN	$MAPbI_3$	23.10	1.01	0.73	17.10	5
NiO_x	$MAPbI_3$	22.38	0.90	0.76	15.38	6
Co_3O_4	$(5\text{-}AVA)_xMA_{1-x}PbI_3$	23.48	0.88	0.64	13.27	7
CuSCN/rGO	$Cs_{0.05}(MA_{0.17}FA_{0.83})_{0.95}Pb(I_{0.83}Br_{0.17})_3$	23.24	1.11	0.78	20.40	8
CuSCN/Spiro	$MAPbI_{3-x}Cl_x$	22.01	1.06	0.77	18.02	9
V_2O_5/NiPc	$(FAPbI_3)_{0.85}(MAPbBr_3)_{0.15}$	23.10	1.08	0.73	18.30	10
NiO_x/Spiro	$(FAPbI_3)_{1-x}(MAPbBr_3)_x$	22.68	1.08	0.70	17.20	11
FBT-Th_4/Cu_xO	$MAPbI_3$	21.77	1.11	0.73	17.74	12
MnS	$(FAPbI_3)_{0.85}(MAPbBr_3)_{0.15}$	23.40	1.11	0.77	19.86	This work

References

(1) Li, X.; Yang, J.; Jiang, Q.; Chu, W.; Zhang, D.; Xin, J. Synergistic Effect to High-Performance Perovskite Solar Cells with Reduced Hysteresis and Improved Stability by the Introduction of Na-Treated TiO_2 and Spraying-Deposited CuI as Transport layers. *ACS Appl. Mater. Interfaces* **2017**, *9*, 41354-41362.

(2) Wu, Q.; Xue, C.; Li, Y.; Zhou, P.; Liu, W.; Zhu, J.; Dai, S.; Zhu, C.;Yang, S. Kesterite Cu_2ZnSnS_4 as a Low-Cost Inorganic Hole-Transporting Material for High-Efficiency Perovskite Solar Cells. *ACS Appl. Mater. Interfaces* **2015**, *7*, 28466-28473.

(3) Nejand, B. A.; Ahmadi, V.; Gharibzadeh, S.; Shahverdi, H. R. Cuprous Oxide as a Potential Low Cost Hole Transport Material for Stable Perovskite Solar Cells. *ChemSusChem* **2016**, *9*, 302-313.

(4) Zhang, H.; Wang, H.; Chen, W.; Jen, A. K. Y. $CuGaO_2$: A Promising Inorganic Hole-Transporting Material for Highly Efficient and Stable Perovskite Solar Cells. *Adv. Mater.* **2017**, *29*, 1604984.

(5) Yang, I. S.; Sohn, M. R.; Sung, S. D.; Kim, Y. J.; Yoo, Y. J.; Kim, J.; Lee, W. I. Formation of Pristine Cuscn Layer by Spray Deposition Method for Efficient Perovskite Solar Cell with Extended Stability. *Nano Energy* **2017**, *32*, 414-421.

(6) Yang, Y.; Chen, H.; Zheng, X.; Meng, X.; Zhang, T.; Hu, C.; Bai, Y.; Xiao, S.; Yang, S. Ultrasound-Spray Deposition of Multi-Walled Carbon Nanotubes on NiO Nanoparticles-Embedded Perovskite Layersfor High-Performance Carbon-Based Perovskite Solar Cells. *Nano Energy* **2017**, *42*, 322-333.

(7) Bashir, A.; Shukla, S.; Lew, J. H.; Shukla, S.; Bruno, A.; Gupta, D.; Baikie, T.; Patidar, R.; Priyadarshi, A.; Mathews, N.; et al. Spinel Co_3O_4 Nanomaterials for Efficient and Stable Large Area Carbon-Based Printed Perovskite Solar Cells. *Nanoscale* **2018**, *10*, 2341-2350.

(8) Arora, N.; Dar, M. I.; Hinderhofer, A.; Pellet, N.; Schreiber, F.; Zakeeruddin, S. M.; Grätzel, M. Perovskite Solar Cells with Cuscn Hole Extraction Layers Yield Stabilized Efficiencies Greater Than 20%. *Science* **2017**, *358*, 768.

(9) Li, M.; Wang, Z. K.; Yang, Y. G.; Hu, Y.; Feng, S. L.; Wang, J. M.; Gao, X. Y.; Liao, L. S. Copper Salts Doped Spiro-OMETAD for High-Performance Perovskite Solar Cells. *Adv. Energy Mater.* **2016**, *6*, 1601156.

(10) Cheng, M.; Li, Y.; Safdari, M.; Chen, C.; Liu, P.; Kloo, L.; Sun, L. Efficient Perovskite Solar Cells Based on a Solution Processable Nickel (II) Phthalocyanine and Vanadium Oxide Integrated Hole Transport Layer. *Adv. Energy Mater.* **2017**, *7*, 1602556

(11) Cao, J.; Yu, H.; Zhou, S.; Qin, M.; Lau, T.-K.; Lu, X.; Zhao, N.; Wong, C.-P. Low-Temperature Solution-Processed NiO_X Films for Air-Stable Perovskite Solar Cells. *J. Mater. Chem. A* **2017**, *5*, 11071-11077.

(12) Guo, Y.; Xiong, L.; Li, B.; Fang, G.; et al. Integrated Organic-Inorganic Hole Transport Layer for Efficient and Stable Perovskite Solar Cells. *J. Mater. Chem. A* **2018**, *6*, 2157-2165